Physics-Informed Simplified Model of a Hall Thruster

IEPC-2024-814

Presented at the 38th International Electric Propulsion Conference, Toulouse, France
June 23-28, 2024

Sarah Burrows,* Ethan Webb,† Jiyansh Agarwal,‡ Karthik Naganathan,§ Christopher McDevitt,¶ and Subrata Roy‖

Applied Physics Research Group, University of Florida, Gainesville, Florida, 32611, USA

Abstract: The dynamics of a Hall thruster are investigated numerically with the novel application of Physics-Informed Neural Networks (PINNs). The efficacy of PINNs is explored as a potential design tool for the purpose of efficiently simulating a simplified form of the original one-dimensional Hall thruster model.[1] Numerical novelty includes the utilization of PINNs, for mesh-less convergence, and stability of the solution. The process of imposing a PINN requires the development of a normalization scheme for all partial differential equations (PDEs) and appropriate boundary conditions. The optimization criteria is the minimization of the residuals of the normalized PDEs as close to true zero as possible via algorithms encompassed in Adam and L-BFGS.[2,3] With the model presented, a small convergence criteria of 10^{-8} was produced, which corresponds to a maximum solution error of $\epsilon \approx 10^{-4}$. This was produced with a convergence time of 4 minutes and 32 seconds with 10,000 collocation points and 40,000 epochs (iterations). Since the results are based to the simplified system of PDEs, it is unreasonable to claim the results presented follow all of the complex physics represented within the Hall thruster. As such, this paper encompasses an intermediate model of six simplified steady state equations for a Hall thruster ignoring the nearwall physics, with a focus of qualitative result analysis to effectively validate the use of PINNs against suitable literature. While the model lacks physical process fidelity, results show reasonable trend of a Hall thruster operating at steady state.

*Graduate Student, NDSEG Fellow, Mechanical and Aerospace Engineering, sarahburrows@ufl.edu
†Graduate Student, Material Science and Engineering, ewebb2@ufl.edu
‡Undergraduate Student, Mechanical and Aerospace Engineering, jiyanshagarwal@ufl.edu
§Graduate Student, Mechanical and Aerospace Engineering, naganathan.k@ufl.edu
¶Associate Professor, Material Science and Engineering, cmcdevitt@ufl.edu
‖Professor, Mechanical and Aerospace Engineering, roy@ufl.edu

Nomenclature

Variables

V	= velocity $\left[\frac{m}{s}\right]$
z	= domain in the axial direction $[m]$
m	= mass $[kg]$
n	= number density $\left[\frac{1}{m^3}\right]$
p_e	= pressure $[Pa]$
e	= electron charge $[C]$
E_z	= electric field $\left[\frac{V}{m}\right]$
E'	= wall loss $[eV]$
Ω	= Hall parameter
ω_{ce}	= electron cyclotron frequency $\left[\frac{1}{s}\right]$
ω_{pe}	= electron plasma frequency $\left[\frac{1}{s}\right]$
ν	= collisional frequency $\left[\frac{1}{s}\right]$
S	= source $\left[\frac{1}{m^3 s}\right]$
α_B	= Bohm diffusion coefficient $\left[\frac{m^2}{s}\right]$
α	= energy loss per ionization
E_I	= ionization energy of xenon $[eV]$
T	= Temperature $[K, eV, J]$
φ	= electric potential $[V]$
t	= time $[s]$
J_T	= total current density $\left[\frac{A}{m^2}\right]$
A	= area $[m^2]$
$\dot{m}$	= mass flow rate $\left[\frac{kg}{s}\right]$
ρ	= density $\left[\frac{kg}{m^3}\right]$
Γ	= flux $\left[\frac{1}{m^2 s}\right]$
σ	= collisional cross-section $[m^2]$
k_i	= ionization process constant $\left[\frac{m^3}{s}\right]$
X	= dummy variable

Subscripts

i	= ion particles
n	= neutral particles
e	= electron particles
ei	= electron-ion particles
en	= electron-neutral particles
in	= ion-neutral particles
w	= wall
z	= along the z-axis
θ	= along the θ-axis
ref	= reference value
0	= initial value

Superscripts

$0+$	= neutral to singly ionized
$\dot{X}$	= time-based derivative
$\bar{X}$	= normalized variable

Acronyms

DSMC	= Direct Simulation Monte Carlo
PIC	= Particle-in-cell
VPIC	= Vector Particle-in-cell
ANN	= Artificial Neural Network
PINN	= Physics-Informed Neural Network
HET	= Hall-Effect Thruster, Hall Thruster

I. Introduction

Hall Thruster experimentation started in the early 1960s, and because of diligent international efforts, became an enabling technology for onboard propulsion in many space applications. This coaxial device consists of four key parts: the anode, which serves as a propellant distributor; an annular acceleration channel made of boron nitride typically; a magnetic unit; and a hollow cathode (see Figure 1).[4]

The magnetic unit comprised of coils induces a radial magnetic field between the thruster center line and the outer edge. Gas is fed into the discharge channel through the anode, while electrons are emitted from the external hollow cathode. Electrons attempt to gravitate towards the positively biased anode, but have their mobility reduced in the axial direction by a transverse radial magnetic field. This effectively traps electrons, creating an acceleration region where neutral atoms are ionized by the electrons through impact ionization. The magnetic field strength is chosen such that the heavier ions accelerate axially through the potential created by the anode and cathode, rather than spiral around the thruster channel. The remaining electrons from the hollow cathode will neutralize part of the ion beam in the exit plume. Present-day Hall-Effect Thrusters (HETs) offer specific impulses over 2000 s, and thrust and power well-exceeding 100 mN and 5 kW, respectively.[5] The HET efficiencies are approximately 50% with operational lifetimes over 10,000 hours.[6]

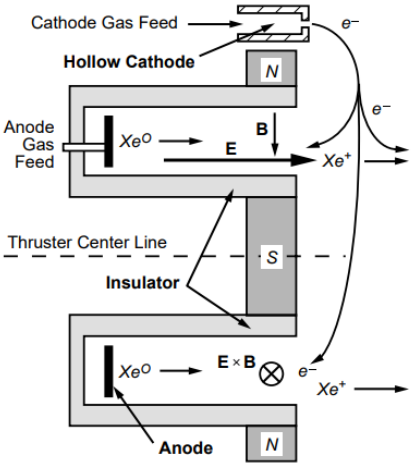

Figure 1: Schematic of a hall thruster, with emphasis on the radial magnetic field and the accelerating electric field[4]

An abundance of experimental data for Hall thruster characterization reveals that there are known discrepancies between ground-testing results and in-flight diagnostics.[7] These measurement differences occur due to a variety of inconsistencies between systems, whether it be facility effects or electrical circuit variations. As construction of an infinitely large vacuum chamber to mimic the space environment is intractable, the physical domain limitations in ground testing always impose unrealistic effects on data collected on the ground. While certain hyper-parameters can be tuned to match in-space conditions, this is still not the most reliable alternative for determining Hall thruster characteristics, as it makes models less reproducible since parameters must change for each different experimental set-up. This allows for the justification of experiment-informed computational methods that possess the ability to numerically represent a variety of Hall thruster configurations. While computational methods cannot replace experimentation, they allow for a cost-effective initial step that enhances the data-based results.

Despite significant numerical and theoretical advances of recent past, there are still several obstacles present in the traditional use of Particle-In-Cell (PIC), hybrid, and fluid models. In the hybrid PIC model, ions and neutrals are treated as particles, while electrons are streaming as fluid. While this enables the inclusion of detailed kinetics from individual particle modeling, PIC methods have significant computational costs. In the fluid formulation, all species are described by their respective macroscopic equations. While this method is not as computationally intensive, the fluid models are typically created on a case-by-case basis, which negatively impacts general application. Several one- and two- dimensional models are available in literature. Manzella,[8] Boeuf and Garrigues,[9] Ahedo *et al.*[10](to name a few in no particular order) have documented one-dimensional Hall thruster simulations. Fife,[11] Keidar *et al.*,[12] and Roy and Pandey[13] document the two dimensional numerical results. Even with their central roles in characterizing HET functions, the employment of these tools is often complicated by the need to incorporate multi-physics, complex geometries, and the treatment of real time analyses.[14] In particular, one especially challenging aspect of Hall thruster modeling is wall interactions with the plasma, including the sheath and pre-sheath region at the walls and anode. This becomes even more daunting as the viscosity and heat flux distribution due to the heavy particles also affect the performance of the high power HETs.[15]

To overcome several of these theoretical challenges and numerical modeling limitations of the previous Hall thruster models, the use of Artificial Neural Networks (ANN) can provide design level efficiency learning from experiment and physics-based models. Furthermore, similar to the standard (PIC/VPIC/DSMC/hydrodynamic) plasma simulation, ANNs can be enhanced with wall processes and interactions present in a physical HET system. The framework used to carry out this approach is called a Physics-Informed Neural Network (PINN).[16]

What separates PINNs from other neural networks is the inclusion of physical equations that constrains

the solution. Furthermore, such a model can be used in a "forward" manner to analyze data, solve the equations directly, or incorporate data to further tune the results. Thus, PINNs are able to bridge the gap between data rich and data poor regimes, allowing for physical solutions despite limited data availability. The final results are anticipated to give an accurate model at a high speed that is versatile. Even though the presented model does not yet have experimental data, the described PINN framework will enable the use of data in the future. While it is expected that the training portion of this model is intensive, once trained, the surrogate model is expected to provide accurate predictions for Hall thruster operation in drastically less computational time compared to other conventional numerical methods. Namely, while the training of a PINN can be substantial, their online inference time is exceptionally short, often on the order of microseconds. Further noting that PINNs can be trained for a broad range of parameters,[17,18] the trained PINN can be used as a rapid surrogate of the Hall thruster performance across a diverse range of thruster designs. A further distinction of PINNs compared to many traditional numerical methods is that PINNs do not require the inclusion of meshing. This prevents the need for mesh convergence, generation, and testing, which is one of many obstacles encountered in mesh-dependent numerical methods.

Without the inclusion of data, the model presented represents that of the forward problem. This serves as an initial step in the model development, since results of the forward problem will demonstrate whether the physics are adequately represented. In this proceeding, the forward problem is developed via the simplification and normalization of the seven equation system presented in Roy & Pandey.[1,19] These simplified equations are then passed through a PINN, which returns the optimized results for most major components in a Hall thruster: electron temperature, electron velocity, ion number density, neutral number density, ion velocity, and electric field, with the exception of neutral velocity. It is important to note that the model presented is simplified to a steady state assumption with a constant neutral velocity. The procedure to model development with wall physics is an incremental process, and the details of the neutral velocity are the last to be included before establishing the forward problem as complete. While the present study focuses on a single design with a given set of parameters, previous work has indicated that extending the model to learn the parametric solution to a system of PDEs does not pose a fundamental challenge.[20,21] Such an extension will be left to future work.

II. Approach: Physics-Constrained Deep Learning

The PINN framework is focused on minimizing the residual of one or more PDEs as well as approximating the solution of the targeted PDE(s) through boundary conditions inputted into a neural network (see equation 1). More specifically, the PDE(s) utilized in this model will align with the steady-state governing equations of a Hall thruster, with the assumptions described subsequently.

An approximate solution is found via solving the optimization problem. As depicted in Figure 2, ANNs are composed of layers of neurons. The first layer is the input layer and the last layer is the output layer. In between are hidden layers, and each has a distribution of weights and biases that are optimized in order to reduce the loss function. This process is done via the use of gradient-descent method and backpropagation: where the adjusting of weights and biases in a neural network is performed by analyzing the error rate from the previous iteration, and then the weights and biases are determined to minimize equation 1.[22] The algorithm works in a backwards-fashion to test for errors from outputs nodes to input nodes.

Ideally, in the final stage of model development, a rapid surrogate model will be produced for predicting the flow characteristics for a variety of input parameters within the Hall thruster. A loss function suitable for this task can be expressed as[23]

$$\text{Loss} = \frac{1}{N_{\text{PDE}}} \sum_{i}^{N_{\text{PDE}}} |R(x_i)|^2 + \frac{\lambda}{N_{\text{bdy}}} \sum_{i}^{N_{\text{bdy}}} |u(x_i) - u_i|^2. \tag{1}$$

where $R(x_i)$ is the residual of the PDE(s), the second term on the right hand side enforces the boundary conditions, and λ is a regularizer that determines the relative importance of the PDE and boundary terms. N_{PDE} and N_{bdy} represent the number of points to sample inside the simulation domain and along the boundary, respectively. If this model were to be extended into a time dependent problem, an additional term would need to be applied to enforce the initial conditions.

A known limitation in the modeling scheme is the complexities of minimizing a loss function comprised of multiple terms. For example, in equation 1, encompassing the physics of the Hall thruster requires multiple PDEs, and thus an added term to the loss function for each PDE. Having more terms in the loss function creates more challenges for convergence in the optimizer.[24]

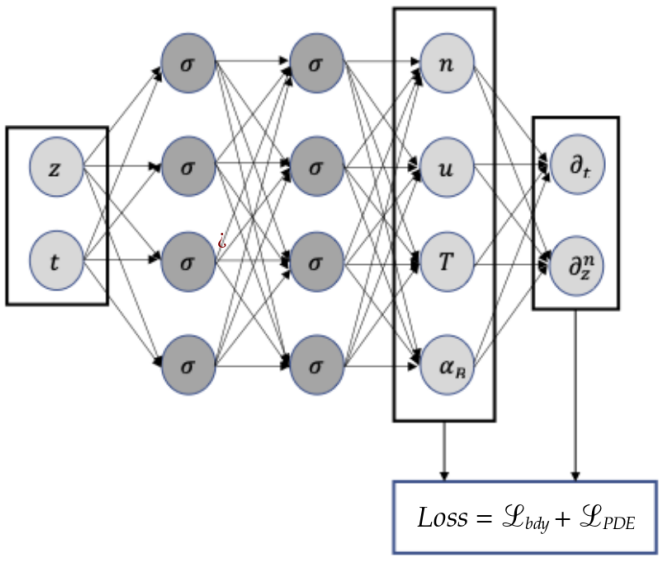

Figure 2: Schematic of the proposed future neural network architecture. The neural network would take (z, t) as inputs, feed it through hidden layers, and output the plasma fields.

Another notable limitation is that the optimizer can fail to exactly satisfy boundary conditions, which results in physically inaccurate solutions. This was overcome by adding a layer after the last hidden layer of the neural network that transforms the output of the hidden layers such that boundary conditions are exactly enforced, thus removing the boundary terms from equation 1. This can be illustrated for the case of a Dirichlet boundary condition: $u(x) = u_{\text{bdy}}(x) + u_{\text{zero}}(x)\, u'(x)$, where $u'(x)$ is the output of the hidden layers of the ANN, $u(x)$ is the predicted solution, and $u_{\text{zero}}(x)$ is created such that this term vanishes on the system's boundaries, allowing $u_{\text{bdy}}(x)$ to satisfy the boundary conditions.

III. Neural Network Architecture

A. DeepXDE

DeepXDE is the primary framework used to produce the results described. This is a python library for scientific machine learning and physics-informed learning that utilizes reputable machine learning libraries such as TensorFlow or PyTorch as a backend.[25] DeepXDE allows for easy construction of network architecture. In light of anticipating future work on this model, DeepXDE allows for the ease of incorporating data as a constraint to the network.

B. Fully-Connected Neural Network

A "Fully Connected" Neural Network (FNN) refers to a neural network in which each input node is connected to each output node. The major advantage of a fully-connected neural network is that they are "structure agnostic".[26] Thus, no special assumptions need to be made about input data types. In addition to this, it has the most documentation and potential sources to reference, allowing for simple implementation.

C. Activation Function: Hyperbolic Tangent

The essence of a neural network lies in the hidden layers where weights and biases can be adjusted to get reasonable outputs via gradient-descent and backpropagation. However, one obstacle with the use of gradient-descent methods is derived from the property that large and smaller numbers can have huge/tiny gradients. The optimizer employs these gradients to know which direction and magnitude to fine-tune weights and biases, which could cause weight and bias terms to either extrapolate to infinity or disappear to zero, respectively. Incorporating an activation function addresses these concerns by constraining weights and biases to be on a reasonable order of magnitude. There are two general types of activation functions:

linear and nonlinear. While linear has its place in numerics, it could not be applied to this problem. Linear activation functions always have the feature where negative numbers stay close to zero, but positive numbers are allowed to grow, which can lead to the exploding gradients problem. Furthermore, many linear activation functions are discontinuous at zero, which would be disastrous for the current application of the gradient-descent method. The notable exception is Exponential Linear Unit (ELU), but that still possesses the potential for exploding gradients.

As such, a nonlinear activation was sought out: the hyperbolic tangent. The benefit of employing the hyperbolic tangent function is that it and its higher order derivatives are continuous and differentiable across it's entire domain. Hyperbolic tangent activation functions specifically allow all values of weights and biases to be confined to [-1, 1]. In addition, the nonlinearity allows the network to be more expressive in its outputs since it can handle nonlinear outputs such as both exponentials and natural logs.

D. Initializer: Glorot Uniform

Within the network of weights and biases, a nontrivial initial condition must be applied to each neuron called the initialization function. The initialization chosen for a model can significantly impact the convergence time for a given simulation. It is effectively like racing in the 100 meter dash, except a proper initialization function would get a 50 meter head-start. Glorot Uniform specifically is a shifted normal distribution for the weight's and bias' initial values. This distribution is conducive to convergence for PINNs and proven to reduce convergence speed.[27] Thus, it is more than suitable for this model.

IV. The Presented Model

A. Physical Processes and Assumptions

The thruster plasma is a partially ionized gas, consisting of electron, ion, and neutral xenon particles. In such a plasma, both elastic and inelastic processes take place simultaneously. Elastic collisions involve only exchange of momentum and energy between colliding particles, whereas inelastic processes can be responsible for redistributing the number density of the particles along with its momentum and energy. That being said, not all processes are equally probable, and only the most imperative processes will be included when applicable. For example, inelastic processes such as recombination, charge-exchange collision, and plasma-wall interactions will not be considered in the present work. Additionally, momentum exchange between electron-electron and ion-ion collisions will not be considered as their relative drift due to charge attraction will be small in comparison to that of the electron-ion collisions. However, the inelastic process of ionization will be included with the approximation that neutral and ion source terms are equal and opposite ($|S_i| \approx |-S_n| = |S|$).

The plasma in the thruster is assumed to be quasineutral (electron and ion number densities are approximately equal: $n_e \approx n_i$), ignoring the thin sheath layers near the anode and cathode. In a similar vein, the masses of ions and neutrals are assumed to be equivalent ($m_i \approx m_n$). Despite the plasma being quasineutral for the duration of the channel length, the electrostatic field is maintained due to the charge separation within the acceleration channel.

B. Problem Geometry

The problem geometry consists of a one-dimensional line that occurs along the center axis of an axisymmetric, cylindrical Hall thruster. A 4.0 centimeter Hall thruster length is assumed, with an area of 0.0045 $[m^2]$.[1,9]

V. The Governing Equations

In order to fully characterize the system, seven key, one-dimensional equations are referenced from Roy & Pandey[1] in the present work: electron momentum, electron energy, ion continuity, ion momentum, neutral continuity, current conservation, and mass conservation. These equations are derived with few assumptions and are dependent on definitions such as collisional frequencies and the ionization source terms, which are defined subsequently. Note that the electron response time is much faster than that of ions due to the higher order of magnitude for electron velocity (V_e). Hence, in Roy and Pandey[1,19] the electron momentum and

energy equations are considered steady-state while for slower ions and neutrals, a set of time-dependencies were included. However, in the simplified present work, these ions and neutrals will also be considered steady.

A. Collisions

1. electron-ion (Coulomb) collisions

Plasma particles are deflected over the Debye length (λ_{De}) due to the long-range nature of the Coulomb force.

$$\nu_{ei} = \frac{4\sqrt{2\pi}}{3\sqrt{m_e}} \frac{e^4 n_i L_e}{T_e^{3/2}} = \frac{L_e}{3\sqrt{2\pi}} \left(\frac{n_i}{n_e}\right) \left(\frac{\omega_{pe}}{n_e \lambda_{De}^3}\right), \tag{2}$$

where $\omega_{pe}^2 = 4\pi n_e e^2/m_e$ is the square of the electron plasma frequency with an electron mass m_e and charge e, $\lambda_{De}^2 = T_e/(4\pi n_e e^2)$ is the square of the Debye length, and $L_e = ln(\Lambda)$ is the Coulomb logarithm. For the context of low-temperature space plasmas, the Coulomb logarithm was selected to have a value of 15.[1] Typical values of L_e are approximately from 10 to 20 where weak-scattering events caused by long-range forces dominate transport properties.

2. electron-neutral collisions

The plasma-neutral collisional frequency is $\nu_{en} = n_n \langle \sigma V_{\text{the}} \rangle$ where V_{the} is the thermalized velocity based off the Maxwell distribution. After calculation, it can be found that electron-neutral collisions can be approximated as $\nu_{en} \approx n_n(2.50 \times 10^{-13})$, which is also in Boeuf.[9] Typically, for a majority of the Hall thruster regime, the effect of Coulomb collisions may be smaller or of the same order of magnitude in comparison with the electron-neutral collisions.

3. ion-neutral collisions

A constant was assumed for ion-neutral collisional frequency based from Roy & Pandey's model. This constant came out to be $\nu_{in} = 1.80 \times 10^6$.[1]

B. Ionization

The inelastic process of electron collisions with a xenon atom is the main source of ion production within a propulsive plasma. The rate of ion production in the plasma is determined via the total cross section of the process. The only collisions considered are the transition from which a neutral becomes a singly ionized state ($Xe^0 \rightarrow Xe^+$), which is represented below.[1] This corresponds to why Coulomb, electron-neutral, and ion-neutral collisional frequencies were considered.

$$S_{\text{ionization}} = k_i^{0+} n_e n_n, \tag{3}$$

where k_i is a process constant, and n_e and n_n correspond to electron and neutral particle number densities, respectively. The function for k_i^{0+} is described for a singly charged ionization as a general third-order temperature-dependent polynomial fitted to experimental data based on the Maxwellian distribution function:[1]

$$k_i^{0+} = (1.9435 \times 10^{-5} T_e^3 - 0.0068 T_e^2 + 0.6705 T_e - 1.6329) \times 10^{-14}; \quad T[eV]. \tag{4}$$

C. Magnetic Field

In a typical Hall thruster experiment, the radial field is dominant in comparison with the axial field. Thus, a one-dimensional radial magnetic field is prescribed based on an adapted Gaussian distribution (see equation 5 and Figure 3), which is scaled to fit the defined 4 cm thruster profile.[9]

$$B = B_{max} \cdot 1.02 \mathrm{e}^{\frac{-(z-0.8)^2}{0.3^2}}, \tag{5}$$

where B_{max} is the maximum magnetic field strength determined to be 200 Gauss, and z is an azimuthal location along the thruster domain.

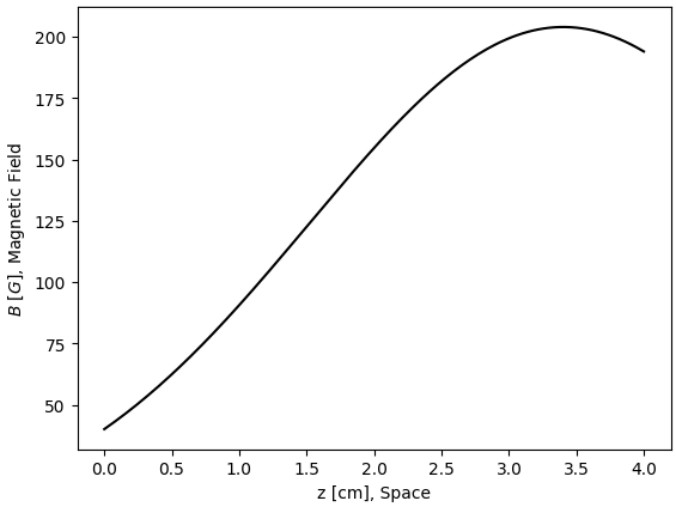

Figure 3: The imposed magnetic field distribution. The magnetic field is maximum upstream of the exit plane.

D. Electron Momentum

With the understanding that the dynamics of the electron are determined primarily by the pressure gradient, electric and magnetic forces, and collisional exchange of momentum, the electron momentum equation can be defined. The presence of Coulomb, electron-neutral, and wall interactions are thought to play an imperative role in electron transport. Thus, they are kept in the governing derivation:

$$\begin{aligned} V_{ez}\frac{\partial V_{ez}}{\partial z} = -\frac{1}{m_e n_e}\frac{\partial}{\partial z}(p_e) - \frac{e}{m_e}E_z - \Omega\omega_{ce}V_{ez} - \nu_{ei}(V_{ez} - V_{iz}) \\ - \left(\frac{S}{n_e}\right)(V_{ez} - V_{nz}) + \nu_w V_{ez}, \end{aligned} \tag{6}$$

where the following relations between azimuthal (V_{ez}) and axial electron velocities ($V_{e\theta}$) are utilized:

$$\Omega = \left(\frac{\omega_{ce}}{\nu_{ei} + \nu_{en} + \alpha_B\omega_{ce}}\right), \tag{7}$$

and

$$V_{e\theta} = \Omega V_{ez}, \tag{8}$$

where, α_B is the Bohm diffusion coefficient, ν_w is the wall collisional frequency, p_e is pressure, and Ω is the Hall parameter. The inclusion of α_B is to qualitatively account for the effect of anomalous Bohm conductivity, which is equivalent to frequency $\nu_B = \alpha_B\omega_{ce}$. The presence of ω_{ce} in this relationship incorporates the effect of magnetic field fluctuations ($\omega_{ce} = 1.76 \times 10^7 B$ where B is in Gauss).

E. Electron Energy

Electron energy is derived to include the effect of Joule heating, random thermal energy exchange, ionization interactions, and plasma interaction with the wall. Neglecting the effects of radiation, viscous dissipation, and thermal conduction, the electron energy equation can be written as:

$$\begin{aligned} \frac{d}{dz}\left\{n_e V_{ez}\left[\frac{m_e(1+\Omega^2)V_{ez}^2}{2} + \frac{5}{2}T_e\right]\right\} - n_e e V_{ez}\frac{d\varphi}{dz} \\ = 3\frac{m_e}{m_i}n_e\nu_{ei}(T_i - T_e) + 3\frac{m_e}{m_n}n_e\nu_{en}(T_n - T_e) \\ + S\left(\frac{3}{2}T_e + \alpha E_I\right) - n_e\nu_w E', \end{aligned} \tag{9}$$

where T_e, T_i, and $T_n \approx 0.3[eV]$ are electron, ion, and neutral temperatures in eV, respectively. E_I is the ionization energy of xenon ($E_I \approx 12.1[eV]$), φ is the electric potential, E' is the wall loss, and α is the collisional excitation energy loss per ionization with a value of $\alpha \approx 2.5$.

F. Ion Continuity

The ion continuity equation is:

$$\frac{\partial n_i}{\partial t} + \frac{\partial (n_i V_{iz})}{\partial z} = S - \nu_w n_i, \tag{10}$$

which occurs in its non-steady-state form.

G. Ion Momentum

In the derivation of ion momentum, particle properties were leveraged to simplify the equation. Ions are considered to be unmagnetized due to their large gyration (Larmor) radius in a 200G magnetic field, and thus the effect of magnetic field on ion transport is neglected. Additionally, the pressure gradient term is ignored as the thermal energy of ions are much smaller than their kinetic energy ($T_i << m_i V_i^2$). These assumptions give the following form for ion momentum:

$$\frac{\partial V_{iz}}{\partial t} + V_{iz}\frac{\partial V_{iz}}{\partial z} = \left(\frac{e}{m_i}\right) E_z + \left(\frac{m_e}{m_i}\right) \nu_{ei}(V_{ez} - V_{iz}) - \left(\frac{m_n}{m_i}\right) \nu_{in}(V_{iz} - V_{nz}) - \left(\frac{S}{n_e}\right)(V_{iz} - V_{nz}) + \nu_w V_{iz}. \tag{11}$$

H. Neutral Continuity

The neutral continuity equation is:

$$\frac{\partial n_n}{\partial t} + \frac{\partial (n_n V_{nz})}{\partial z} = -S_n, \tag{12}$$

which also occurs in its non-steady-state form. The source term for neutrals is equal and opposite to that defined in equation 3.

I. Current Continuity

Current conservation serves a supplementation to equations 6-12:

$$e n_i (V_{iz} - V_{ez}) = J_T, \tag{13}$$

where

$$J_T = \frac{I_d}{A}. \tag{14}$$

J_T is the total current density, I_d is the total discharge current, and A is the cross section of the thruster channel.

J. Mass Conservation

Mass conservation is shown as:

$$m_n n_n V_{nz} + m_i n_i V_{iz} = \frac{\dot{m}}{A}, \tag{15}$$

where

$$\dot{m} = \rho V A. \tag{16}$$

$\dot{m}$ is the mass flow rate, which encompasses neutral, ion, and electron flow.

VI. Simplified Governing Equations to be Applied to the Model

The primary challenge with implementing a PINN in this context is the debugging process for creating a hall thruster model. This is an iterative process that can take significant time to develop a final working model. In the presented work, 6 out of 7 equations from Roy and Pandey[1] have been implemented in simplified form and the neutral continuity equation assumes a constant neutral velocity.

Each governing equation solves for a different variable within the presented system. More specifically: (i) the electron momentum equation determines electric field, (ii) the electron energy equation determines electron temperature, (iii) the ion continuity equation determines ion number density, (iv) the ion momentum equation determines ion velocity, (v) the neutral continuity equation determines neutral velocity, (vi) the current continuity equation determines electron velocity, and (vii) the mass conservation equation determines neutral number density.

There is only one direct input into the neural network: the dimensional space z. The neural network outputs correspond to the number of partial differential equations being solved for in the described equation set. With the simplification of neutral continuity, that leaves four PDEs which each include spatial derivatives, and three algebraic equations. Algebraic equations are not directly passed through the optimizer, but rather imposed as hard constraints to the equation system. Even though the network will only directly see the PDEs, the algebraic equations (current continuity, neutral continuity, and mass conservation) will still play a role in solution determination and optimization since all equations are coupled.

A. Electron Momentum Simplified

From equation 6, electron inertia was assumed to be small and negligible. In addition, the pressure gradient and wall collisional terms are most influential near walls and sheaths, neither of which are incorporated in this model.

$$0 \approx -\frac{e}{m_e}E_z - \Omega\omega_{ce}V_{ez} - \nu_{ei}(V_{ez} - V_{iz}) - \nu_{en}(V_{ez} - V_{nz}) - \left(\frac{S}{n_e}\right). \tag{17}$$

B. Electron Energy Simplified

Much of equation 9 is neglected, as they are not important outside of the wall and sheath regions.

$$\begin{aligned}\frac{d}{dz}\left(n_e V_{ez}\frac{5}{2}T_e\right) - n_e e V_{ez}\frac{d\varphi}{dz} \approx 3\frac{m_e}{m_i}n_e\nu_{ei}(T_i - T_e) + 3\frac{m_e}{m_n}n_e\nu_{en}(T_n - T_e) \\ +S\left(\frac{3}{2}T_e + \alpha E_I\right).\end{aligned} \tag{18}$$

C. Ion Continuity Simplified

The assumption of steady-state is applied to ion continuity in equation 19 as this is only a one-dimensional problem. Additionally, wall collisions are also neglected.

$$\frac{\partial(n_i V_{iz})}{\partial z} \approx S. \tag{19}$$

D. Ion Momentum Simplified

The assumption of steady-state is also applied to ion momentum in equation 20 as this is only a one-dimensional problem. Wall collisional terms are also neglected.

$$V_{iz}\frac{\partial V_{iz}}{\partial z} \approx \left(\frac{e}{m_i}\right)E_z + \left(\frac{m_e}{m_i}\right)\nu_{ei}(V_{ez} - V_{iz}) - \left(\frac{m_n}{m_i}\right)\nu_{in}(V_{iz} - V_{nz}) - \left(\frac{S}{n_e}\right)(V_{iz} - V_{nz}). \tag{20}$$

E. Neutral Continuity Simplified

As the iterative process is still ongoing for model development, Neutral Continuity is reduced to its simplest form to ease modeling. Although this means that the model is not yet complete at the time of this proceeding, an approximation will still allow the physical solution to show qualitative trends towards the later expected high-fidelity solutions.

$$V_{nz} \approx Constant. \tag{21}$$

F. Current Continuity Simplified

No further assumptions are applied to the derivation of current continuity.

$$en_i(V_{iz} - V_{ez}) = J_T. \tag{22}$$

G. Mass Conservation Simplified

From equation 16, the mass of neutrals and ions are approximated to be equivalent. Additionally, mass flow rate is approximated to neglect electron mass flow.

$$m_n n_n V_{nz} + m_i n_i V_{iz} \approx m_n(\Gamma_n + \Gamma_i) \approx \frac{\dot{m}}{A}, \tag{23}$$

where Γ is the flux of a given particle.

VII. Normalized Equations

In order for the system of equations to be compatible with the machine learning network, they must be normalized. The goal of this normalization is to transform each equation to be on a similar scale with respect to each other. This, in turn, improves the performance and training stability of the machine learning model. Otherwise, the PINN will run into convergence-preventative obstacles such as exploding gradients for large terms, or the wrongful neglect of terms on a smaller order of magnitude in comparison.

A. Normalization Scheme

The reference values for normalization are given in Roy & Pandey and are defined as follows:[1]

$$\begin{gathered}\Gamma_{ref} = 10^{23} m^{-2} s^{-1},\ T_{ref} = E_i[12.1eV],\ V_{ref} = \sqrt{\frac{T_{ref}}{m_i}} m s^{-1},\ n_{ref} = \frac{\Gamma_{ref}}{V_{ref}} m^{-3},\ \nu_{ref} = \sigma_{ref}\Gamma_{ref} s^{-1}, \\ \sigma_{ref} = \sigma_0 \left(\frac{m_i}{m_e}\right)^{\frac{1}{2}},\ z_{ref} = \frac{V_{ref}}{\nu_{ref}},\end{gathered} \tag{24}$$

where

$$\sigma_0 = 3.6 \cdot 10^{-20} m^2. \tag{25}$$

The normalization can then be performed with respect to these reference parameters defined in equation 24:

$$\bar{X} = \frac{X}{X_{ref}}, \tag{26}$$

where X can be any variable of choice such as z, V_i, n_i, etc.

A useful conversion for φ and T_{ref} was applied to allow for the following:

$$\bar{\varphi} = \frac{\varphi}{T_{ref} = \varphi_{ref}[eV]} = \frac{\varphi}{eT_{ref}[J]}. \tag{27}$$

B. Normalization Technique

To normalize each equation properly, it is imperative to ensure that each equation remains balanced. Each term, which is comprised of variables such as n, V, etc. must have the same units as the next term within the same equation. This known property is useful for determining what normalization coefficient must be used for an entire PDE.

1. Ion Momentum Equation Normalized

From the simplified ion momentum equation, the term with the least complexity is selected to determine the normalization factor for the entire equation. Any term is viable, this is simply the most robust approach to normalization and unit determination.

$$V_i \frac{\partial V_i}{\partial z}. \tag{28}$$

Within equation 28, it can be seen that there are two primary variables: V_i and z. As such, the normalization references provided above ($z = \bar{z} z_{ref}$ and $V_i = \bar{V}_i V_{ref}$ from equation 26) can be applied to equation 28. This gives the following:

$$V_i \frac{\partial V_i}{\partial z} \left(\frac{z_{ref}}{V_{ref}^2} \right) = \bar{V}_i \frac{\partial \bar{V}_i}{\partial \bar{z}}. \tag{29}$$

This is the normalized version of the ion inertia term, and this coefficient z_{ref}/V_{ref}^2 can be used as the normalization factor for every other term in the ion momentum equation. This is shown below.
The electric field term becomes:

$$\frac{e}{m_i} E_z \rightarrow -\frac{e}{m_i} \frac{\partial \varphi}{\partial z} \left(\frac{z_{ref}}{V_{ref}^2} \right) = -\frac{\partial \bar{\varphi}}{\partial \bar{z}} = \bar{E}_z. \tag{30}$$

For the collisional terms, the reference equation for z_{ref} is applied to find a relationship between z, V, and ν. Then the normalization of electron-ion (Coulomb) and ion-neutral collisions become:

$$\left(\frac{m_e}{m_i} \right) \nu_{ei} (V_{ez} - V_{iz}) \rightarrow \left(\frac{m_e}{m_i} \right) \nu_{ei} \left(\bar{V}_{ez} - \bar{V}_{iz} \right) \frac{1}{\nu_{ref}}, \tag{31}$$

$$\left(\frac{m_n}{m_i} \right) \nu_{in} (V_{iz} - V_{nz}) \rightarrow \left(\frac{m_n}{m_i} \right) \nu_{in} \left(\bar{V}_{iz} - \bar{V}_{nz} \right) \frac{1}{\nu_{ref}}. \tag{32}$$

Lastly, the source term normalization relies on number density. As such, the normalization scheme can be adapted to become the equivalent: $\frac{z_{ref} n_{ref}}{V_{ref}^2 n_{ref}}$. This allows for number density to be accounted for, without changing the normalization scheme.

$$\left(\frac{S}{n_e} \right) (V_{iz} - V_{nz}) = \frac{k_i^{0+} n_n n_e}{n_e} (V_{iz} - V_{nz}) \rightarrow k_i^{0+} \bar{n}_n (\bar{V}_{iz} - \bar{V}_{nz}) \frac{z_{ref} n_{ref}}{V_{ref}}. \tag{33}$$

Now, the ion momentum equation can be written as the following in its final form:

$$\bar{V}_i \frac{\partial \bar{V}_i}{\partial \bar{z}} = \bar{E}_z + \left(\frac{m_e}{m_i} \right) \nu_{ei} \left(\bar{V}_{ez} - \bar{V}_{iz} \right) \frac{1}{\nu_{ref}} - \left(\frac{m_n}{m_i} \right) \nu_{in} \left(\bar{V}_{iz} - \bar{V}_{nz} \right) \frac{1}{\nu_{ref}} - k_i^{0+} \bar{n}_n (\bar{V}_{iz} - \bar{V}_{nz}) \frac{z_{ref} n_{ref}}{V_{ref}}. \tag{34}$$

2. Ion Continuity Equation Normalized

From the simplified ion continuity equation, the term with the least complexity is again selected to normalize:

$$\frac{\partial (n_i V_{iz})}{\partial z}. \tag{35}$$

Within equation 35, it can be seen that there are three primary variables: V_i, n_i, and z. As such, the normalization references provided above ($z = \bar{z} z_{ref}$,$n_i = \bar{n}_i n_{ref}$, and $V_i = \bar{V}_i V_{ref}$ from equation 26) are applied. This gives the following:

$$\frac{\partial (n_i V_{iz})}{\partial z} \left(\frac{z_{ref}}{n_{ref} V_{ref}} \right) \rightarrow \frac{\partial (\bar{n}_i \bar{V}_{iz})}{\partial \bar{z}}. \tag{36}$$

Lastly, the source term is dependent on two number densities, which necessitates there being two reference number densities in the normalization scheme. In order to achieve this the normalization is adapted to look like the following: $\left(\frac{z_{ref} n_{ref}}{V_{ref} n_{ref}^2} \right)$. Normalizing the source term with this factor gives:

$$S = k_i^{0+} n_n n_e \rightarrow k_i^{0+} n_n n_e \left(\frac{z_{ref} n_{ref}}{V_{ref} n_{ref}^2} \right) = k_i^{0+} \bar{n}_n \bar{n}_e \frac{z_{ref} n_{ref}}{V_{ref}}. \tag{37}$$

This gives ion continuity in its final form as:

$$\frac{\partial \bar{n}_i \bar{V}_{iz}}{\partial \bar{z}} = k_i^{0+} \bar{n}_n \bar{n}_e \cdot \left(\frac{z_{ref}}{V_{ref} n_{ref}} \right). \tag{38}$$

3. Neutral Continuity Equation Normalized

The value for normalized neutral velocity is assumed to be given. This value was approximated through Roy & Pandey's numerical results.[1]

$$\bar{V}_{nz} \approx 0.4. \tag{39}$$

4. Electron Momentum Equation Normalized

Following the same normalization scheme as the ion momentum equation, the final normalized form of the electron momentum equation becomes:

$$0 \approx -\frac{m_i}{m_e} \bar{E}_z - \Omega \omega_{ce} \bar{V}_e \frac{1}{\nu_{ref}} - \nu_{ei} (\bar{V}_e - \bar{V}_i) \frac{1}{\nu_{ref}} - \nu_{en} (\bar{V}_e - \bar{V}_n) \frac{1}{\nu_{ref}} - \left(k_i^{0+} \bar{n}_n \right) (\bar{V}_e - \bar{V}_n). \tag{40}$$

This result can be achieved due to both momentum equations possessing the same units.

5. Current Continuity Equation Normalized

Despite this equation being labeled as a continuity equation, the units are different than what is described in ion continuity. As such, the normalization scheme for continuity as described in Section 2 cannot be applied. Following the same process as described prior, the normalization factor for the equation is:

$$e n_i \left(V_i - V_e \right) \rightarrow e n_i \left(V_i - V_e \right) \frac{1}{n_{ref} V_{ref}} = e \bar{n}_i \left(\bar{V}_i - \bar{V}_e \right). \tag{41}$$

After applying this scheme to the rest of the equation, current continuity in its final form becomes:

$$e \bar{n}_i \left(\bar{V}_i - \bar{V}_e \right) = J_T \frac{1}{n_{ref} V_{ref}} = \frac{I_d}{A} \frac{1}{n_{ref} V_{ref}}. \tag{42}$$

6. Mass Conservation Normalized

Following the same process for mass conservation gives:

$$m_n n_n V_n \rightarrow m_n n_n V_n \frac{1}{n_{ref} V_{ref}} = m_n \bar{n}_n \bar{V}_n. \tag{43}$$

With the simplified configuration, mass does not need to be normalized as it will cancel out with the mass terms embedded in mass flow rate:

$$\bar{\dot{m}} = m_n \bar{V}_n \cdot \bar{n}_{n0} - m_i \sqrt{\frac{T_e}{T_{ref}}} \cdot \bar{n}_i, \tag{44}$$

where $\sqrt{\frac{T_e}{T_{ref}}}$ is the normalized ion velocity $\bar{V}_i$.
Applying this normalization scheme to the rest of the equation gives the following:

$$\bar{n}_n = \frac{\bar{\dot{m}} - \bar{n}_i \bar{V}_i}{\bar{V}_n}. \tag{45}$$

7. Electron Energy Equation Normalized

Similar to all approaches prior, the normalization factor is found:

$$\frac{5}{2} \frac{\partial}{\partial z} \left(n_e V_{ez} T_e \right) \rightarrow \frac{5}{2} \frac{\partial}{\partial z} \left(n_e V_{ez} T_e \right) \cdot \frac{z_{ref}}{n_{ref} V_{ref} T_{ref}} = \frac{5}{2} \frac{\partial}{\partial \bar{z}} \left(\bar{n}_e \bar{V}_{ez} \bar{T}_e \right). \tag{46}$$

Applying this to the rest of the equation through similar techniques gives electron energy in its final form:

$$\frac{5}{2} \frac{\partial}{\partial z} \left(\bar{n}_e \bar{V}_{ez} \bar{T}_e \right) + \bar{n}_e \bar{V}_{ez} E_z = 3 \frac{m_e}{m_i} \bar{n}_e \nu_{ei} (\bar{T}_i - \bar{T}_e) \frac{1}{\nu_{ref}} + 3 \frac{m_e}{m_n} \bar{n}_e \nu_{en} (\bar{T}_n - \bar{T}_e) \frac{1}{\nu_{ref}}. \tag{47}$$

VIII. Conditions Prescribed to the Model

A. The Physics Layer

In order to improve the robustness of the PINN, a tailored layer between the hidden layers of the neural network and the eventual output is introduced. This 'physics layer' will enforce several properties of the solution as hard constraints such as (i) positivity of quantities such as density and temperature, (ii) boundary conditions at $z = 0$, (iii) the potential drop across the thruster, and (iv) enable several of the underlying equations to be exactly satisfied at $z = 0$. While such properties could be enforced as additional terms in the loss function, by enforcing them as hard constraints this will limit the space of solutions that the optimizer searches across. This will be shown below to have the effect of improving the robustness of the PINN. The physics layer presented has the following properties:

1. The neutral number density at the inlet is assumed as given and equal to the reference number density (n_{ref}). This is not applied within the output transform as the algebraic mass conservation equation's residual is not being optimized.

2. Ion number density is determined based on Roy & Pandey's condition of $n_{i0} = 0.014 \cdot n_{ref}$.[1] The output transform is as follows: $n_i = n_{i0} + n_1 \tanh\left(\frac{z}{L} \cdot n_{i,NN}^2\right)$, where $n_{i,NN}$ corresponds with the associated hidden layers output for ion number density and n_1 corresponds to a maximum ion number density.

3. The constraint for electric field was set such that a voltage drop was enforced across the thruster, noting the relationship $E_z = -\frac{\partial \varphi}{\partial z}$. The output transform is written in terms of electric potential and is as follows:
$\varphi = \varphi_0 \cdot \frac{(L-z)(L+z)}{L^2} - \frac{\varphi_1 z}{L}\frac{(L-z)}{L} + \left(\frac{z}{L}\right)^2 \cdot \varphi_{NN}$,
where φ_{NN} corresponds with the associated hidden layers output for electric field, $\varphi_0 = 100V$ is an initial electric potential, and φ_1 is the derivative of φ.

4. Physics layer condition for ion velocity is chosen such that the ion momentum equation (see equation 34) is exactly satisfied at $z = 0$: $V_i = k_0^+ \cdot n_{n0}/\nu_{ref} \cdot z + V_{i,Max} \tanh((\frac{z}{L})^2 \cdot V_{NN})$, where V_{NN} corresponds with the hidden layers output associated with ion velocity.

5. The electron temperature is assumed to be equivalent to $T_{e0} = 3.0[eV]$ at the inlet. The output transform is as follows: $T_e = T_{e0} \cdot e^{\frac{z}{L} \cdot T_{e,NN}}$, where $T_{e,NN}$ corresponds with the associated hidden layers output for electron temperature.

From conditions 1-5 it is apparent that at $z = 0$, the ion density, velocity and temperature satisfy $n_i = n_{i0}$, $T_e = T_{e0}$, and $V_i = 0$, which are the boundary conditions for these fields. Thus, regardless of the output of the hidden layers of the neural network, the boundary conditions will be automatically satisfied. It is also apparent that the ion density and temperature are guaranteed to be positive definite [see conditions for ion number density (item 2) and electron temperature (item 5)]. Furthermore, the parameter n_1 is set to define the maximum density that the optimizer will search for, thus preventing the optimizer from looking for unphysically large ion densities. In practice, n_1 should be chosen to be substantial so that the range of solutions considered isn't artificially restricted, but small enough to restrict the network to physically plausible values of the density. The performance of the PINN is not sensitive to the precise value of this parameter.

From condition 3 it is apparent that the electrostatic potential is equal to $\varphi = \varphi_0$ at $z = 0$ and $\varphi = 0$ at $z = L$, regardless of the value of φ_{NN}. This then guarantees that a potential drop of φ_0 across the axial dimension is enforced. Finally, the prefactors of conditions ion velocity and electric potential were chosen to ensure that the ion continuity and momentum equations are exactly satisfied at $z = 0$ (item 4). Specifically, the first derivatives of V_i and φ are forced to be equal to:

$$\left.\frac{\partial V_i}{\partial z}\right|_{z=0} = k_0^+ \cdot n_{n0}/\nu_{ref}, \tag{48}$$

$$\left.\frac{\partial \varphi}{\partial z}\right|_{z=0} = \varphi_1, \tag{49}$$

which results in the ion continuity and momentum equation being exactly satisfied at $z = 0$. By guaranteeing that the first derivative of V_i and φ are exact at $z = 0$, this forces the solution to be accurate for small

values of z, and thus further improving the robustness in the training of the PINN. Without enforcing this property, the residual of the system of ODEs was found to be maximal at $z = 0$. By enforcing exact first derivatives of a subset of fields at $z = 0$ results in the residual of two ODEs vanishing identically at $z = 0$, with only modest residuals for the other two ODEs, as illustrated Section IX,.

B. Conditions to Introduce Flexibility into the Model

A known challenge with modeling Hall thruster physics is the stiffness of the equations prescribed. In order to mitigate this challenge, the model was given flexibility in what it was able to select for current density. Furthermore, the model was set up such that a potential drop is enforced of $\varphi_0 = 100V$, with which discharge current could then be computed from. This is what is performed in several models such as Boeuf[9] and Ahedo,[10] and is referred to as a trainable variable. Consequently, the model is able to train and select the value for current density that best suits the physics provided. As a result, model stiffness was reduced and convergence improved.

IX. Results and Discussion

It is important to emphasize that since the model is still undergoing the iterative debugging process, these results do not fully encompass the physics represented within the Hall thruster described in Roy & Pandey.[1] Even though this is the case, these results still provide a general precursor as to whether or not PINNs are a viable tool to use in the electric propulsion community.

The described equation set has been solved numerically over a computational domain of the channel length with the exit plane located at 4cm. No meshing was required to achieve these results or solutions. The neural network architecture includes one input (z), four outputs (PDE residuals), four hidden layers, and 32 neurons per layer. There is no determinate method to select the number of hidden layers for a neural network, but making this value proportional to the number of outputs was conducive for model convergence while balancing computational cost. The network tested 10,000 collocation points per epoch, with 40,000 epochs. More specifically, the Adam optimizer operated for the initial 10,000 epochs to start the training process, and then L-BFGS trained for the remaining 30,000 epochs. The learning rate, similar to a time-step of sorts, for both of these algorithms was 10^{-4}. The training process took an approximate 4 minutes and 32 seconds.

The trainable variable of total current density referenced in Section B resolved to a value of 6.5859A. During model development, it was noted that if the current density was prescribed by the user rather than determined by the potential drop, convergence would not be met at higher amperage. This is a point of concern within the model and will be explored further in future work.

A. Output Results

1. Loss History

In additional efforts to debug the model and conclude on the viability of PINNs, residual plots were made versus space as well as versus epoch. Plotting residuals versus space for the last epoch in the training process is advantageous as they allow for conclusions to be drawn regarding where the network is facing the most challenges in the domain. Typically, the model encounters these points on the boundaries if there are discrepancies in the physics application. Ideally, the residual versus space should oscillate about true zero. Plotting residuals versus epoch allows for conclusions to be drawn on the error of the model with respect to the physics it was provided. What is considered to be excellent convergence criterion is an error of $\epsilon < 10^{-3}$, where residual relates to the square of error (residual $= \epsilon^2$)

Figure 4 demonstrates the loss history versus epoch, which demonstrates how well the optimizers were able to converge with each iteration. It can be seen that the convergence criterion is surpassed with the lowest residual being on the order of to 10^{-8}, which corresponds to an error of 10^{-4}. This, with the added clarity given by the residual plots versus space, serve as the final indicator that the results provided have converged to capture the relevant physics. This, however, does not guarantee accuracy of the solution as this is a simplified model.

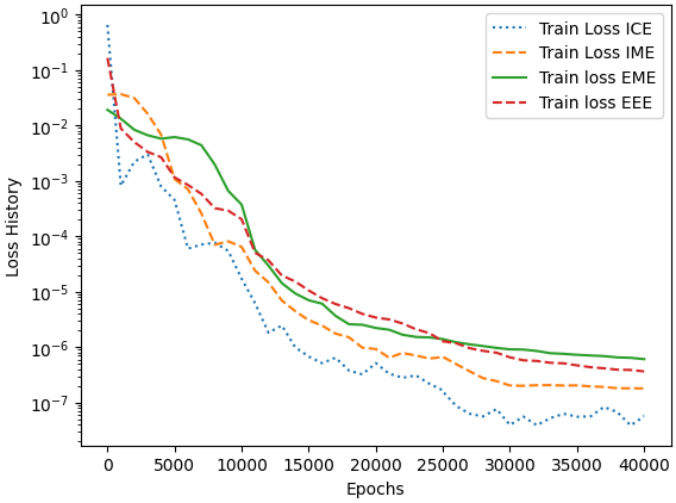

Figure 4: Convergence of each optimized PDE versus epoch. ICE stands for the Ion Continuity Equation, IME represents the Ion Momentum Equation, EME corresponds to the Electron Momentum Equation, and EEE denotes the Electron Energy Equation.

2. *Ion Continuity and Mass Conservation Equations (n_i and n_n)*

In Figure 5, it can be seen that the ion continuity residual trained optimally. The residual oscillates about true zero for the entire span of the domain. Although the residual is largest in amplitude at the thruster inlet and exit, the order of magnitude is small and thus not a point of concern.

The rapid increase in ion number density (from 0.35×10^{18} to 1.25×10^{18}) correctly corresponds to the rapid decrease in neutral number density (from 2.0×10^{19} to 0.05×10^{19}), as represented in Figures 6 and 7. This is qualitatively consistent with the fact that as neutrals enter the thruster chamber they undergo impact ionization, thus turning neutrals into ions. In reality, ion number density should not decrease almost an order of magnitude from the maximum density to the thruster exit. Additionally, neutral number density should not decrease on the magnitude with which is occurring. However, the trends and physical concepts validate what is undergone in a Hall thruster despite these discrepancies.[1] The input parameter of $\varphi_0 = 100V$ is expected to have a significant affect on results. Similar to the model failing to converge for higher amperage inputs, the model also fails to converge for larger potential drops. This is due to the direct correspondence between thruster power, voltage drop, and current. The lower input potential was required to reach convergence criteria with the truncated model, even if the value of $100V$ isn't considered standard operating conditions.

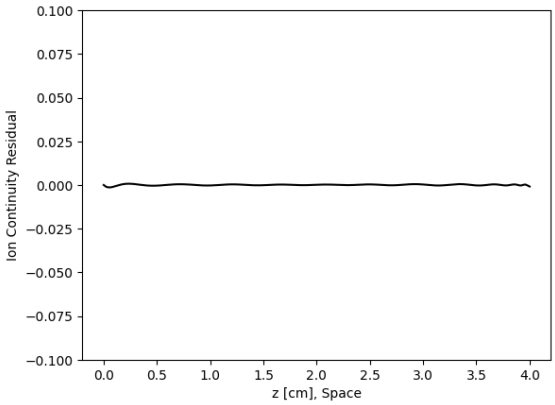

Figure 5: The residual for the ion continuity equation plotted versus thruster domain.

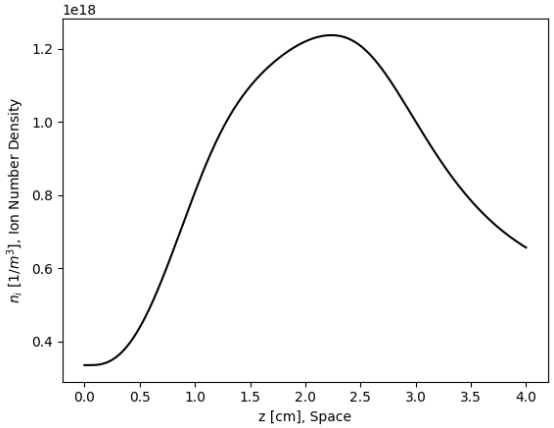

Figure 6: Numerical Solution for ion number density throughout the thruster domain.

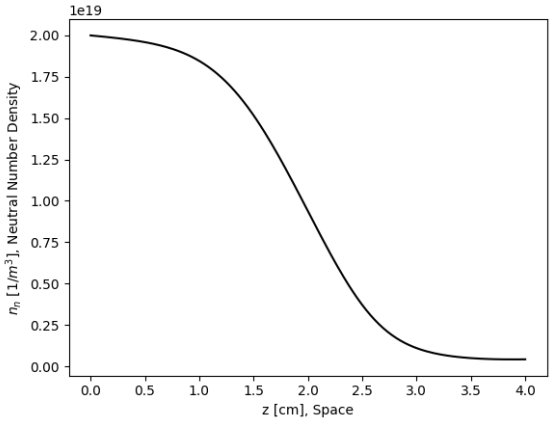

Figure 7: Numerical Solution for neutral number density throughout the thruster domain.

The location of peak ion number density is validated by Figure 8, where the maximum ionization corresponds with maximum ion number density. This denotes the ionization region within the Hall thruster model.

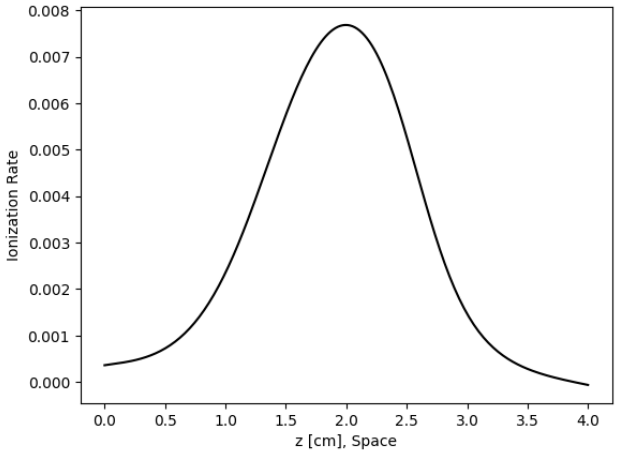

Figure 8: Numerical Solution for ionization rate throughout the thruster domain.

3. Ion Momentum and Current Continuity (V_i and V_e)

In Figure 9 it can be seen that the residuals are optimal as well. Figure 10 describes the axial ion velocity profile. The peak ion velocity occurs at the end of the domain, but the steepest gradients are from regions 10mm to 20mm. This denotes the acceleration region of the model. Ions are accelerated primarily due to the presence of the potential gradient, which is at a maxima near the channel exit. This lack of true maxima at the end of the domain could be attributed to the relatively small prescribed initial potential compared to what is denoted in Roy & Pandey (100V vs. 300V).[1] In reality, the maximum ion velocity would peak and then decay at the thruster exit.

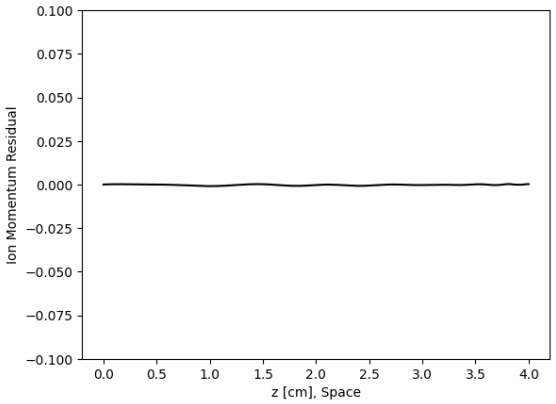

Figure 9: The residual for the ion momentum equation plotted versus thruster domain.

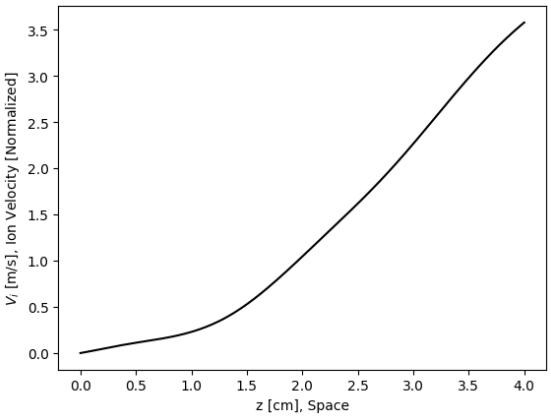

Figure 10: Numerical Solution for ion velocity throughout the thruster domain.

The results associated with the electron velocity profile are consistent to the provided conditions, but not consistent with performance in a Hall thruster. In theory, the electron velocity should start small in magnitude and increase within the acceleration region due to the presence of the magnetic field peaking in this region. However, this is ongoing investigative work, and shortcomings of this solution are likely a result of the reduced model.

Even with these graph discrepancies, it can still be seen qualitatively that the model is finding a solution close to what represents a Hall thruster. The PINN faced little trouble when converging this simplified model, so it is unreasonable to conclude that convergence problems will occur when the model is complete. Any and all discrepancies, as such, are proven to be a product of the reduced-physics model and boundary conditions provided in-code, which will be relaxed in future iterations.

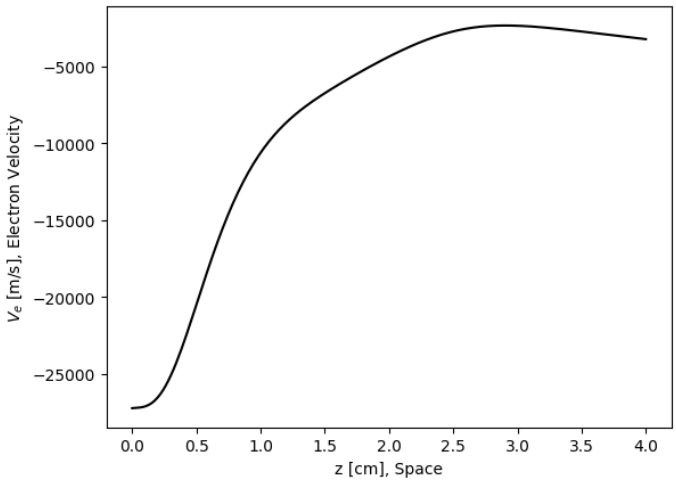

Figure 11: Numerical Solution for electron velocity throughout the thruster domain.

4. Electron Momentum (E_z)

In Figure 12, it can be seen that the electron momentum equation converged properly with minimal residual variance versus space. Figure 13 denotes the electric field, which is the negative gradient of potential, φ. The peak occurring in this plot is consistent with what occurs in literature, but the ascent begins sooner than what is standard.[1]

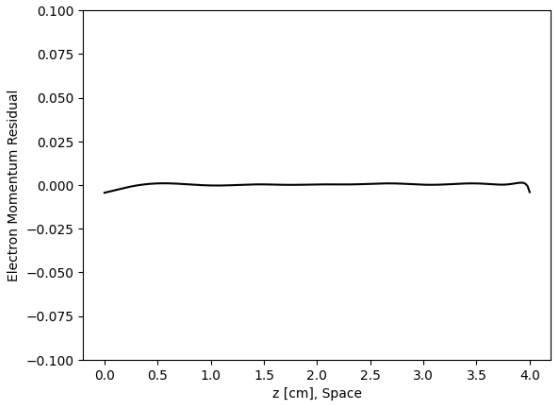

Figure 12: The residual for the electron momentum equation plotted versus thruster domain.

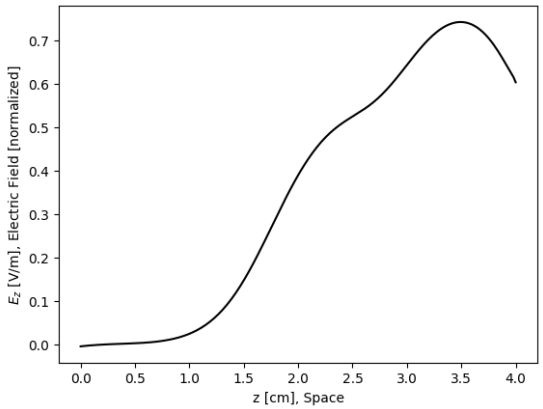

Figure 13: Numerical Solution for electric field throughout the thruster domain.

5. *Electron Energy*

Figure 14 shows that, throughout the bulk of space, the residuals oscillate about zero. There are discrepancies in oscillation period and amplitude, but none of these values significantly vary from true zero to justify a point of concern. Figure 15 describes the electron temperature profile. The increase in the temperature is not uniform in the channel, which is consistent with literature.[1] The maximum increase occurs approximately three-quarters into the thruster channel. For the presented model, the magnitude of the electron temperature maxima is higher than what is found in Roy & Pandey.[1] In theory, the peak in electron temperature can be attributed to ohmic heating and maximum gyration energy in this region. However, this does not appear to be the case for this model. This could point to some apparent limitations of the present one-dimensional simplified model.

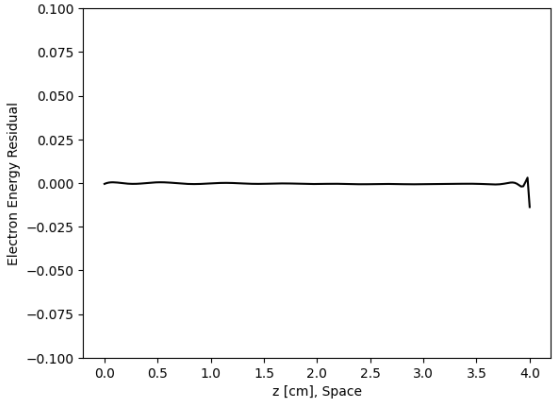

Figure 14: The residual for the electron energy equation plotted versus thruster domain.

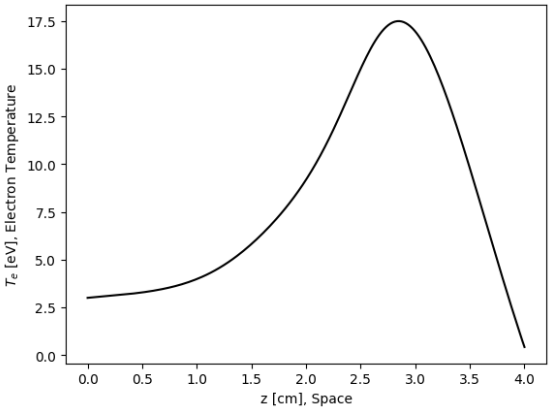

Figure 15: Numerical Solution for electron temperature throughout the thruster domain.

X. Conclusion

In this paper, a simplified, steady, one-dimensional PINN model is presented for a Hall thruster with quasineutral plasma. The model includes the formulation of partially ionized plasma using the multi-component fluid equations to study the convergence and solutions PINNs can produce to validate viability.

The plasma and neutral density profiles are in decent agreement with reported literature. The ion density subsequently is also in decent agreement as these parameters are inversely related. The electron temperature and electric field profile predict a maximum in the downstream region of the Hall thruster. The axial ion velocity distribution shows that ions are accelerated down the channel, as would be expected for a thruster plasma.

While the PINN implementation was relatively successful, the presented one-dimensional model had several simplifying assumptions, which limited the proper validation of the results. Specifically, the electron and ion momentum equations were simultaneously considered at steady state which severely limits the accuracy of the solution. The neutral velocity needs to be calculated, and reasonable wall loss terms should be brought back to recover proper physical processes described in reference literature.[1,14,19] This is one of the final steps remained in the model development before considering the addition of anode fall or incorporating experimental data.

A. Future Work

Upon addition of the neutral continuity equation into the system and relaxing simplifications, the fluid model will become complete. In the future, relationships between the initial electric potential, current density, and convergence rates will be further explored. As of now, the model faces difficulty in training at larger input discharge voltages and input amperages. These future results are also expected validate the use of PINNs, allowing the problem to then be extended to multiple dimensions with higher-order parameter space simulations that are not presently possible with conventional methods. With the addition of a modest quantity of experimental data, the neural network can be expanded such that it can accurately predict solutions over a variety of thruster configurations at low computational cost. This is implemented via an additional term in the loss function by replacing N_{bdy} by N_{data} in equation 1, where N_{data} represents the number of data points utilized. The addition of data will greatly extend the neural network's ability to predict dominant characteristics that arise in a Hall thruster. As such, this research has the novelty and potential to grow and be improved upon to positively contribute to the electric propulsion community.

Acknowledgements

S. K. Burrows thanks the National Defense Science and Engineering Graduate Fellowship program for funding this work. Additionally, authors would like to extend our deepest appreciation to Dr. Christine Greve of the In-Space Propulsion Branch of the AFRL and Dr. Mark Scherbarth of the Space Vehicle Directorate of the AFRL for their support throughout.

References

[1]S. Roy and B. P. Pandey, "Plasma-wall interaction inside a hall thruster." *Journal of Plasma Physics*, vol. 68, pp. 305–319, 2002.

[2]D. Kingma and J. Ba, "Adam: A method for stochastic optimization," *International Conference on Learning Representations*, 2014.

[3]Y. Xiao, Z. Wei, and Z. Wang, "A limited memory bfgs-type method for large-scale unconstrained optimization," *Computers Mathematics with Applications*, vol. 56, pp. 1001–1009, 2008.

[4]D. Goebel and I. Katz, *Fundamentals of Electric Propulsion: Ion and Hall Thrusters*. JPL Space Science and Technology Series, 2008.

[5]J. M. Haas, F. S. Gulczinski, A. D. Gallimore, G. G. Spanjers, and R. A. Spores, "Performance characteristics of a 5 kw laboratory hall thruster," *American Institute of Aeronautics and Astronautics, Inc.*, 1998.

[6]D. Manzella, J. Yim, and I. Boyd, "Predicting hall thruster operational lifetime," *Proceedings of the 40th AIAA/ASME/SAE/ASEE Joint Propulsion Conference and Exhibit, Fort Lauderdale, FL, USA*, 2004.

[7]W. Hargus and M. Nakles, "Hall effect thruster ground testing challenges," AFRL, Tech. Rep., 2009.

[8]D. Manzella, *Proceedings of the 24th International Electric Propulsion Conference*, vol. 1, p. 277, 1995.

[9]J. P. Boeuf and L. Garrigues, "Low frequency oscillations in a stationary plasma thruster," *Journal of Applied Physics*, vol. 84, pp. 3541–3554, 1998.

[10]E. Ahedo, P. Martínez-Cerezo, and M. Martinez-Sanchez, "One-dimensional model of the plasma flow in a hall thruster," *Physics of Plasmas*, vol. 8, pp. 3058–3068, 2001.

[11]J. Fife, "Hybrid-pic modeling and electrostatic probe survey of hall thrusters," Ph.D. dissertation, MIT, 1999.

[12]M. Keidar, I. Boyd, and I. Beilis, "Plasma flow and plasma–wall transition in hall thruster channel," *Physics of Plasmas*, vol. 8, pp. 5315–5322, 2001.

[13]S. Roy and B. P. Pandey, "Development of a finite element method based hall thruster model for sputter yield predictions," *Proceedings of the 27th International Electric Propulsion Conference*, p. 049, 2001.

[14]F.Taccogna and L.Garrigues, "Latest progress in hall thrusters plasma modelling," *Reviews of Modern Plasma Physics*, vol. 3, p. 12, 2019.

[15]A. Shashkov, A. Lovtsov, D. Tomilin, and D. Kravchenko, "Numerical study of viscosity and heat flux role in heavy species dynamics in hall thruster discharge," *Plasma Sci. Technol.*, vol. 25, p. 015511, 2023.

[16]M. Raissi, P. Perdikaris, and G. Karniadakis, "Physics-informed neural networks: A deep learning framework for solving forward and inverse problems involving nonlinear partial differential equations," *Journal of Computational Physics*, vol. 378, pp. 686–707, 2019.

[17]L. Sun, H. Gao, S. Pan, and J.-X. Wang, "Surrogate modeling for fluid flows based on physics-constrained deep learning without simulation data," *Computer Methods in Applied Mechanics and Engineering*, vol. 361, p. 112732, 2020.

[18]C. J. McDevitt, "A physics-informed deep learning model of the hot tail runaway electron seed," *Physics of Plasmas*, vol. 30, no. 9, p. 092501, 09 2023.

[19]S. Roy and B. P. Pandey, "Numerical investigation of a hall thruster plasma," *Physics of Plasmas*, vol. 9, pp. 4052–4060, 2002.

[20]C. J. McDevitt and X.-Z. Tang, "A physics-informed deep learning description of Knudsen layer reactivity reduction," *Physics of Plasmas*, vol. 31, p. 062701, 2024.

[21]J. S. Arnaud, T. Mark, and C. J. McDevitt, "A physics-constrained deep learning surrogate model of the runaway electron avalanche growth rate," *Accepted to Journal of Plasma Physics (arXiv preprint arXiv:2403.04948)*, 2024.

[22]R. Hecht-Nelsen, "Theory of the backpropagation neural network," *Neural Networks for Perception*, pp. 65–93, 1992.

[23]C. McDevitt, E. Fowler, and S. Roy, "Physics-constrained deep learning of incompressible cavity flows," in *AIAA SCITECH 2024 Forum*, 2024, p. 1692.

[24]Y.-J. Gong, W.-N. Chen, S.-H. Zhan, J. Zhang, Y. Li, Q. Zhang, and J.-J. Li, "Distributed evolutionary algorithms and their models: A survey of the state-of-the-art," *Applied Soft Computing*, vol. 34, pp. 286–300, 2015.

[25]L. Lu, "Deepxde." [Online]. Available: https://deepxde.readthedocs.io/en/latest/index.html

[26]B. Ramsundar and R. B. Zadeh, *TensorFlow for Deep Learning: From Linear Regression to Reinforcement Learning*, 1st ed. O'Reilly Media, Inc., 2018.

[27]X. Glorot and Y. Bengio, "Understanding the difficulty of training deep feedforward neural networks," *Journal of Machine Learning Research - Proceedings Track*, vol. 9, pp. 249–256, 2010.